

DESIGN AND MODELING OF AN ELECTROSTRICTIVE INCHWORM ACTUATOR

A. Suleman¹, S. Burns and D. Waechter²

University of Victoria

Department of Mechanical Engineering

Victoria, B.C., V8W 3P6, Canada

Abstract

Currently, there is a strong and increasing demand for electric actuators. Applications include the automotive, aircraft and space industries. The paper presents a proof-of-concept design of a large displacement and medium force inchworm actuator. The technology considered uses an electrostrictive mechanism that “walks” inside an outer casing. This motion emulates an inchworm, summing small steps to achieve large displacements. The detailed design of the electrostrictive inchworm actuator was performed using finite element analysis. A prototype was constructed and tested and the performance matched well with the numerical simulation results.

1. INTRODUCTION

Over the past decade, new fields of engineering have emerged from a surge of invention and innovation, led by multifunctional materials. In particular, the emerging science of multifunctional materials has spurred progress in the engineering field to enhance the performance of structural systems. The new technologies have invited us to revise the engineering rules, not only because they spur new industries but also because they

¹ IDMEC-IST, Principal Investigator, Corresponding author; Tel: 250-721 6039; Fax: 250-721 6051; E-mail: suleman@uvic.ca

² Sensor Technology Ltd, Collingwood, ON, Canada; Tel: 705-444 1440; Fax: 705-444 6787

embody a sweeping capacity to lower the weight and cost of designing and manufacturing new structural systems while improving overall performance.

Electromagnetic linear actuators have existed for decades. This device delivers limited stroke and force as the total energy is restricted by the electrical energy stored in the coil. In addition, the device is rather bulky, expensive, limited in frequency (due to large inertia) and presents a potential safety hazard in the case of a power failure.

There are several key technological developments that have combined to establish the potential feasibility of electrical actuator systems. One of the advances is the development of functional materials and their utilization in devices such as distributed actuators and sensors. The other development comes from the field of electrical engineering, with the advent of new algorithms and signal processing technologies. The pursuit of advanced materials with multifunctional properties has opened up new horizons in terms of actuation simplicity, compactness and miniaturization potential. The most recognized types of materials are shape memory alloys, magnetostrictive materials and piezoelectrics, which develop strains (or displacements) when exposed to thermal, magnetic and electric fields, respectively.

The electrostrictive phenomenon is a nonlinear property which exists in all dielectric materials. Some of these materials can offer higher electrically induced strains with lower hysteresis than piezoelectric materials. The strain is proportional to the square of the applied electric field and independent of its polarity. The most promising electrostrictive material is lead magnesium niobate (PMN); however, this material is still not widely available on the commercial market. Constitutive models for electrostrictors are not as mature as models for piezoelectrics, due to the non-linearities.

Piezoelectric behavior can be manifested in two distinct ways. The direct piezoelectric effect occurs when a piezoelectric material becomes electrically charged when subjected to a mechanical stress. As a result, these devices can be used to detect strain, movement, force, pressure, or vibration by developing appropriate electrical responses, as in the case of force and acoustic sensors. The converse piezoelectric effect occurs when the piezoelectric material becomes strained when placed in an electric field. The ability to induce strain can be used to generate a movement, force, pressure, or vibration through the application of a suitable electric field. The most promising commercial piezoelectric materials are lead zirconate titanate (PZT) and polyvinylidene fluoride (PVDF).

PZT's offer low strains (~0.06%) with significant hysteresis (~15-20%), whereas electrostrictive PMN materials exhibit higher strains (~0.1%) with lower hysteresis (~1-4%). However, the temperature operating limits for PMN would require that it be specially insulated. For all other considerations, PMN would be handled similarly to PZT and actuator designs for one material could be applied to the other. While PZT is a preferred material for most applications, future commercial applications may favor a direct replacement of PZT with PMN because of its increased strain capabilities and superior hysteresis efficiency. However, piezoelectrics have high bandwidths, they are more compact than magnetostrictive devices and they are bi-directional, unlike electrostrictives.

The potential now exists for electric actuators to deliver high forces over large displacements. Larger displacements can be achieved by stacking piezoelectric or electrostrictive elements. These actuators are being used in micro-positioning xy-tables,

ultrasonic motors, impact printer heads, vehicle suspensions, and precision machining equipment [2-5].

The application of electric field controlled actuators has also been addressed in a variety of space structures applications. Primary attention has been given to research in the area of variable geometry truss structures [6-10]. For example, electrostrictive actuators are used in the correction of the aberrations in the Hubble Telescope. Variable geometry truss structures can adopt a wide range of geometric configurations by lengthening or shortening some of their active elements, each containing a strain-induced actuator. This ability allows these structures to adopt configurations that maximize their structural strength. These structures may also use strain-induced actuators to produce damping effects to suppress vibrations [11,12]. This technology has been integral to many space truss systems including large span roof trusses, space reflectors, and robotic arms [6]. Other applications include release mechanisms, positioning devices, shape control of large flexible surfaces, dexterity and obstacle avoidance [13].

1.1. Past Inchworm Designs

During the last 40 years of development, piezoceramic inchworm actuators have concentrated around a common theme. This theme incorporates piezoceramic stacks for gripping and extending which create the actuator motion. In 1964, Stibitz [14] used a magnetostrictive material on the end of three rods. Each of the three rods would grip, release or push the inner shaft in a predetermined sequence that would actuate the shaft. McNancy [15] developed an amplification device consisting of a piezoceramic stack that was specially positioned against ball bearings. The displacement of the piezoceramic was transferred and amplified through the ball bearings. In 1966, Hsu [16]

designed an actuator using a hollow cylinder with an inner clamping and extending device.

In 1967, Locher [17] developed a mechanism that used two cams to grip and release an inner shaft. The center shaft contained a piezoceramic material producing the extension.

In 1968, Brisbane [18] invented an inchworm actuator using a tube and an inner crawler. The crawler had three piezoceramic elements: two for gripping and one for extension. In 1972, Galutva [19] designed an actuator, which consisted of several piezoceramic elements used for gripping and extending.

In 1975, Bizzigotti and May [20] introduced an inchworm actuator that used curved surfaces to grip the outside of a shaft. The piezoceramic on one end would grip the shaft while the center piezoceramic would extend. After extension, the piezoceramic on the other end would grip the shaft to capture the displacement. In 1976, Sakitani [21] invented the inchworm actuator that would clamp and extend on a surface providing a precise displacement.

In 1979, Ishikawa [22] developed an actuator incorporating the use of two extending and two clamping piezoceramic elements. When energized in a particular sequence the upper shaft would be forced to move horizontally. In 1980, O'Neill [23] presented the first stacked piezoceramic actuator. The idea of stacking increased the actuator displacement. The design involved a cylindrical tube with an inside crawler. In 1984, Taniguchi [24] presented an actuator that used an outer cylindrical shell and an inner crawler. The inner crawler consisted of several cylindrical piezoceramic elements connected together. The firing sequence of the cylindrical piezoceramics was such that a “rippling” motion of extending and clamping made the inner body move. In 1986, Hara

[25] modified the design of Bizzigotti and May by incorporating stacked piezoceramics to increase the actuation displacement. In 1986, Staufenberg [26] created an actuator capable of translational and rotational motion. Many piezoceramics were used in the design. Some were used to grip the shaft while others were used to push the shaft outward (translational motion), or to push the shaft sideways (rotational motion). In 1988, Fujimoto [27] filed a patent consisting of two similar inchworm actuators that use an inner crawler to creep inside a channel.

In 1990, Murata [28] used one set of piezoceramics to engage a shaft with an extremely small pitch. Once engaged, the shaft would be actuated by another set of piezoceramics. In 1991, Shibuta et al. [29] designed an actuator for precise pointing and vibration suppression for anticipated use on the Geostationary Platform planned by NASDA. In 1994, Rennex [30] used piezoceramics with flexure clamps to hold and actuate the inner shaft. In 1996, Pandell and Garcia [31] designed an actuator similar to the design of Galutva but having one extra stage for extension and clamping. In 1997, Galante [32] designed an actuator having an inner shaft that would move with respect to the outer casing. The inner shaft had one piezoceramic used for extension, while the outer casing had two piezoceramics used for gripping. Firing the piezoceramics in a special sequence forced the inner shaft to move. In 1999, Canfield et al. [33] developed an actuator for minimally invasive surgery. The proposed mechanism consists of an inchworm that moves a set of jaws (machined from titanium by the wire EDM process). When the inchworm moves back and forth the jaws are forced to clamp and unclamp. Also in 1999, Frank et al. [34] developed an inchworm for flow control.

Unfortunately, many of these designs rely on extremely high tolerances ($\sim 2.54\mu\text{m}$) with no method of adjustment. In the case of Frank et al. [34], for example, the clearance between output shaft and the gripping surface is less than $5\mu\text{m}$. This exceptionally high tolerance makes the actuator extremely delicate. Any tiny imperfections in machining results in significant loss of performance or prevent actuator motion entirely. Furthermore, most of the inchworm actuators are patented ideas and there has not been an effort to study in detail the design to provide real proof-of-concept performance data. The only designs that have reported performance results are the actuators proposed by Pandell and Garcia with an output force of 13N and a static holding force of 44N with a maximum speed of 1mm/s. The gripping device proposed by Canfield et al. produced a block force of 44N and also a maximum speed of 1mm/s at a frequency of 100Hz.

This paper proposes an improved design and proof-of-concept for an electrostrictive inchworm actuator. The design is based on the actuator's ability to maintain a locked position with no electrical power, fewer number of parts to reduce manufacturing complexity, and its adjustability. The design goals of the actuator are to meet the performance specifications presented in Table 1.

2. ACTUATOR DESIGN AND MODELING

The inchworm actuator concept uses small incremental steps to attain large displacements. This motion is achieved by a mechanism that “crawls” inside an outer casing, as illustrated in Fig. 1. The walking mechanism consists of two flextensional brake assemblies separated by a center electrostrictive stack. Each brake assembly is forced to clamp and unclamp in a particular sequence to capture the displacement of the

center stack. Consequently, the brake assemblies are the most critical aspect of the actuator design.

2.1. The Actuator Stacks

The amount of strain produced in a piezoceramic (piezoelectric or electrostrictive material) is dependent on the thickness of the element and the magnitude of the voltage applied across the thickness. To increase the amount of displacement, many thin piezoceramic elements can be stacked on top of each other. In this stack arrangement, the total stack displacement is equal to the number of elements multiplied by the displacement of each element:

$$\delta_3 = d_{33} E_3 t n \quad (1)$$

where δ_3 is the zero load deflection, d_{33} is the piezoelectric charge coefficient, E is the electric field, t is the thickness of each stack wafer, and n is the number of wafers

The stack is made of electrostrictive material manufactured by Sensor Technology Ltd. [35]. Construction of a stack is achieved by gluing many “wafers” of active material on top of one other. Before the wafers are ready for stack assembly, they must be individually fired, silvered, and poled. The wafers must be protected from excessively high temperatures that will cause the active material to de-pole. The stacks are then encased in a protective wrapping. Lead wires protrude from the encasing for electrical connection. Metal washers are placed at each end to evenly distribute the load to the brittle ceramic. Loads must be compressive and perfectly centered to not damage the stacks.

Using the manufacturer's suggested voltage of 200V with a stack wafer thickness of 0.508mm, the electrostrictive material yields an electric field of 0.3937MV/m. The corresponding strain is 0.0567% (or 2.88×10^{-5} mm per stack element). Using these values, the calculated d_{33} is equal to $0.000567/0.3937 \times 10^6 = 1440$ pC/N. The extending stack of the inchworm has 133 layers (0.381mm each) and a total height of 76.2 mm. This stack provides a displacement of 39.9 μ m when subjected to 200V. table 2 presents a comparative analysis of the free displacement between the piezoelectric and electrostrictive stacks. As observed, the free displacement for the electrostrictive stacks is approximately four times greater than the piezoelectric stacks.

2.2 The Flextensional Frame

The flextensional frames are designed to have an interference fit with the outer casing. When the brake stacks are energized, the frames are forced to distort and reduce in width. This action frees the flextensional frames and allows them to move freely within the outer casing. When the stacks are de-energized, the frames grip the outer casing locking the actuator in place.

Firing each stack in a predetermined sequence creates the actuator motion. First, the left piezo stack is energized. This action compresses the pre-stress material and forces the diagonal arms connected to the brake pads to move up and in; this action releases the top brake pads. Next, the center stack is actuated, pushing the top brake assembly upward. Afterward, the left stack is de-energized, forcing the brake pads to grip the outer casing. The right stack is then fired, releasing the pads. Subsequently, the center stack is de-energized, moving the right brake assembly up. Finally, the right stack is

de-energized, forcing the pads to grip the outer casing and capture the displacement. This sequence is repeated in rapid succession emulating the movement of an inchworm.

The material for the flextensional frame was chosen to have a coefficient of thermal expansion similar to that of the electrostrictive stack to minimize the thermal effect so as to reduce any temperature dependant dimensional variation between the stack and the surrounding material.

The metals chosen must have a high Young's modulus to efficiently transfer the stack force to the brake pads, and a coefficient of thermal expansion similar to the selected actuator stack material. The materials with the highest Young's modulus are oil hardened tool steel, stainless steel 304, and titanium (6% Al, 4%V). The titanium was chosen, however, because it is the closest match to the coefficient of thermal expansion of the piezoceramic ($\sim 1 \times 10^{-6}/\text{C}$). Moreover, titanium (6%Al, 4%V) has a high strength to weight ratio (density = $4730 \text{Kg}/\text{m}^3$).

A rod with adjusting nuts has been inserted through the center of the actuator. In this design, each brake assembly incorporates two pre-stressing adjustments: one for the stack and one for the frame. As shown in Figure 2(a), when adjustment nuts 1 and 2 are tightened, the stack is pre-stressed. This ensures the stacks always remain in compression. When adjustment nuts 1 and 3 are tightened, the frame is pre-stressed. Pre-stressing the frame allows a fine width adjustment within the outer casing.

2.3 Parametric Optimization

The dimensions were broken down into two categories: the fixed dimensions and the free dimensions.

Fixed Dimensions

The fixed dimensions were set due to the size and shape of the electrostrictive stacks quoted from the manufacturer. These stacks have an outer diameter of 25.4mm, an inner diameter of 6.35mm, and height of 57.15mm. The resulting fixed dimensions are shown in Fig. 2(b).

The minimum clearance required to adjust Nut 2 was 10mm. The pre-stress on the PMN stack was chosen to be 4.45N/mm^2 as this is significantly lower than 40N/mm^2 , which is the maximum compressive loading for typical piezoceramic stacks [36]. The last fixed dimension was the threaded rod diameter. It was chosen to be 4.7625mm since it was the next nominal size smaller than the PMN stack hole of 6.35mm.

Free Dimensions

The free dimensions are presented in Figure 2(c) The dimensions having the greatest impact on the design were selected first. The order in which the dimensions were examined is the following: notch thickness (NT), shoulder thickness (ST), arm thickness (AT), arm angle (AA), notch diameter (ND), and casing pre-stress (CP).

2.2. Performance Criteria

To assist in the selection of the free dimensions, three performance criteria were defined: the range, the block force and the fatigue safety factor, as outlined next.

The Range

Referring to Fig. 3(a), when adjustment nut 3 is tightened, the flextensional frame bows outward and the brake pad moves out to position “A”. Now energizing the PMN stack forces the threaded rod to lengthen allowing the flextensional frame to move inward to position “B”. The distance between brake pad locations “A” and “B” is defined as the “range”. The range is important because it is a measure of the brake pad movement during actuation. Too small a range may not allow the brake pad to free itself from the outer casing.

The Blocked Force

The brake pad blocked force is related to the actuator output force through the coefficient of friction constant “ μ ” defined by $F_{out} = 2 * \mu * N$, where F_{out} is the actuator output force, μ is the static coefficient of friction, and N is the brake pad blocked force. The coefficient of friction constant “ μ ” is dependant on many factors such as material, counter-material, lubrication, temperature, speed, loading force, surface finish, surface finish of the counter-material, and type of motion (reciprocating, rotating). Published values can have large variations and range from 0.05 to 0.90. The inside crawler is made from titanium and the outside casing can either be made from titanium or oil hardened tool steel. A typical value is 0.65 for titanium against steel and 0.38 for titanium against titanium [37]. Using these values the actuator output forces are presented in Table 3. For reduced cost of machining and increased frictional force the material choice for the prototype is oil hardened tool steel.

For the brake pad to come in and out of contact, the outer casing must be located somewhere between the maximum and minimum brake pad lateral displacements. To

ensure the brake pads release from the outer casing during actuation there should be a clearance. The minimum suggested clearance is $25.4\mu\text{m}$. To make certain the pad release, the design aims for a clearance between $25.4\mu\text{m}$ and $50.8\mu\text{m}$. For the brake pad to come in and out of contact, the outer casing (“C”) must be located somewhere between “A” and “B”, as shown in Fig. 3(b).

Suppose the PMN stack was energized, and the location of the outer casing “C” was positioned at “B”. The brake pad and the outer casing would be in contact but without force. If the PMN stack was now de-energized, the flextensional frame would try to flex back to position “A” but would be stopped by the outer casing. The normal force exerted on the outer casing is coined the “zero clearance blocked force”.

The Fatigue Safety Factor

The operation of the actuator requires the flextensional frame to bend back and forth a high number of cycles. Each cycle induces a fluctuating stress, which over time may result in the possibility of fatigue failure. To safeguard against this, a fatigue analysis was performed. Using the modified Goodman relation [38], along with the surface roughness taken as machined, the allowable stress amplitude was calculated. Subsequently, the actual stress amplitude was also determined for each design. Dividing the allowable stress amplitude by the actual stress amplitude gives the fatigue safety factor. Investigating the possible locations for fatigue failure it was determined that the most critical location was at the center notches.

The maximum and minimum Von Mises stresses were analyzed. Using these upper and lower limits of stress, a fatigue analysis was performed. The modified Goodman relation rearranged for σ_a is presented in Eq. (2),

$$\frac{\sigma_a}{S_e} + \frac{\sigma_m}{S_{ut}} = 1 \quad (2)$$

where σ_a is the stress amplitude, S_e is the endurance limit, σ_m is the mean stress, S_{ut} is the ultimate stress and

$$\sigma_a = S_e * \left(1 - \frac{\sigma_m}{S_{ut}}\right) \quad (3)$$

The minimum (σ_{min}) and maximum (σ_{max}) stresses were evaluated. The mean stress (σ_m) was then calculated using Eq. (3),

$$\sigma_m = \frac{(\sigma_{max} + \sigma_{min})}{2} \quad (4)$$

Using this value of mean stress (σ_m) in Equation (3) with the endurance limit of machined titanium ($S_e = 279\text{MPa}$) and the ultimate strength of titanium ($S_{ut} = 900\text{MPa}$) yields the maximum allowable stress amplitude ($\sigma_a = \sigma_{allow}$). Now, using the minimum (σ_{min}) and maximum (σ_{max}) stresses the actual stress amplitude (σ_{act}) is determined using:

$$\sigma_{act} = \frac{\sigma_{max} - \sigma_{min}}{2} \quad (5)$$

Finally the “Fatigue Safety Factor” is calculated by dividing the allowable stress amplitude by the actual stress amplitude as:

$$S.F. = \frac{\sigma_{allow}}{\sigma_{act}} \quad (7)$$

Investigating all the possible locations for fatigue failure it was determined that the most critical location was at the center notches of the flextensional frame.

2.3. Results

The parametric analysis results are quite extensive. For illustrative purposes, some representative graphs and trends are shown in Figures 4 and 5.

Notch Thickness (NT): the first and most sensitive dimension that was studied was the notch thickness. To study the notch thickness all dimensions were fixed (to an initial guess at the best design) while only the notch thickness was varied. The notch thickness was varied from 0.75mm to 2mm. The design goal of the brake assembly aims for a range of not less than 90 μ m, a blocked force of over 15N (on each brake pad), and a fatigue safety factor greater than 2.5. A range of 90 μ m should provide adequate adjustment should there be any slight tolerance inconsistency when the design is prototyped. A minimum force of 15N on each brake pad will generate a 30N normal force on the outer casing. This force multiplied by the coefficient of friction for the outer casing material ($\mu_{steel\ on\ Ti} = 0.69$) will lead to a acceptable actuator pushing force of 20.7N. A fatigue factor of safety over 2.5 will safeguard against the high number of cycles the design must endure over its lifetime. Choosing a notch thickness of 1.00mm gives acceptable values for the range, the blocked force, and the fatigue safety factor.

Shoulder Thickness: The next dimension that was considered was the shoulder thickness. Again, all the dimensions were fixed except the shoulder thickness which was varied from 5mm to 10mm. Increasing the shoulder thickness favorably increases both the range and the blocked force; unfortunately, the weight, and the actuator length also increase. A tradeoff between these parameters was met by selecting a shoulder thickness of 9mm.

Arm Thickness: The thickness of the arms was examined next. The arm thickness was varied from 4mm to 8mm. Increasing the thickness of the arms increases range and blocked force, but decreases the fatigue safety factor. A compromise between these variables was chosen by selecting the arm thickness to be 5mm.

Arm Angle: The next free variable that was studied was the arm angle (AA). The angle was varied from 1.19° to 9.42° . Interestingly, as the angle of the arm increases past 3.49° , the range begins to decline. Analyzing the points before and after $AA=3.49^\circ$ shows the arms undergo a “snap through” condition. This means for angles of AA less than 3.49° ($AA < 3.49^\circ$) the arms are concave where as at angles above 3.49° ($AA > 3.49^\circ$) the arms are convex. If the arm angle was chosen to be 3.49° the range would be at its maximum of $109\mu\text{m}$ with the a resulting blocked force of 28N (clearance=50.8N) and the fatigue safety factor of 2.9. However, if the arm angle was chosen to be 4.87° the range would be decreased slightly to $106\mu\text{m}$ along with a decrease in the fatigue safety factor to 2.8, but the blocked force would be drastically increased to 39N. Therefore, the angle of the arm was chosen to be 4.87° .

Notch Diameter: The next free variable that was tested was the notch diameter. The notch diameter was varied from 1mm to 3mm. The notch diameter has little effect on the range or blocked force. Therefore, the notch thickness was chosen to be 2.5mm to ensure a acceptable value of 3.3 for the fatigue safety factor.

Casing Pre-Stress: the last free variable that was investigated was the casing pre-stress. The casing pre-stress was varied from 400N to 800N. The range, blocked force, and fatigue safety factor decrease as the casing pre-stress is increased. Therefore, it is desirable to have a low casing pre-stress. However, the casing pre-stress must not be so low that Nut 3 comes out of contact with the outer casing during actuation. Choosing a casing pre-stress of 565N provides a force of 206N between Nut 3 and the casing during actuation. Note that for adjustment Nut 1 the positive force is taken downward where as for adjustment Nuts 2 and 3 the positive force is taken upward. The dimensions of the brake assembly for the final design are shown in Fig. 6.

3. ACTUATOR PROTOTYPE AND TESTING

A prototype of the computer model was built to attain physical measurements to validate the final design of the actuator. To accomplish this, the procedure was performed in three steps: the assembly of the inner crawler, the manufacturing of the outer casing and the design of the controller. Upon completion of each component of the actuator, the prototype was assembled and tested.

3.1. The Prototype

A pictorial representation of the stacks can be seen in Fig. 7. Two brake stacks and one extending stack were used to assemble the inner crawler.

The inner crawler is assembled from two flextensional frames, two brake stacks, one center stack, and a center rod with adjustment nuts to hold everything together, as shown in Fig. 8. Because the flextensional frames have a complex geometry and need to be manufactured with a tolerance of $12.7\mu\text{m}$, Electro Discharge Machining (EDM) was the chosen manufacturing method. This process cuts each solid block of titanium using a fine copper wire passing a high voltage enabling tolerances up to $2.54\mu\text{m}$.

It should be noted that the prototype frame has extra protrusions (called, guide bumps) along its outer perimeter. These protrusions were an after thought to help keep the inner crawler aligned within the channel during operation. Since the guide bumps are located in regions of low stress, they will not cause any significant discrepancies with the computer model results.

After the flextensional frames were machined, the inside crawler was ready for assembly. To accomplish this, the components were fitted onto the threaded rod and pre-stressed using the adjustment nuts. In order to apply the proper pre-stress the nuts are tightened using a two step sequence.

Initially, Nut 3 is loose and the stack is not energized. Choosing a pre-stress of 565N , Nut 1 and Nut 2 are tightened to a value of 2676N , while Nut 3 remains loose. Now, Nut 1 is tightened against Nut 3 to a value of 565N . The action of tightening Nut 1 and Nut 3 reduces the force between Nut 1 and Nut 2 to a value of 2111N . The corresponding pressure on the stack is therefore $4.45\text{N}/\text{mm}^2$, (which is the recommended pre-stress by the manufacturer [35]).

The nuts on the center stack are also tightened to a value of 2111N to achieve a stack pre-stress of 4.45N/mm². To apply the correct pre-stress the necessary tightening torque was evaluated using:

$$T = \frac{Fd_r}{2} \left(\frac{\tan \lambda + \mu_r \sec \alpha}{1 - \mu_r \tan \lambda \sec \alpha} \right) + \frac{F\mu_p d_n}{2} \quad (7)$$

where T is the tightening torque, F is the pre-stress force, d_r is the mean diameter of threaded rod, μ_r is the coefficient of friction on nut threads, λ is the thread lead angle, α is the thread angle, μ_p is the coefficient of friction of nut surface against the stack, and d_n is the outer mean diameter of nut.

The rod is made from titanium with a 10-32 thread ($d_r = 4.318 \times 10^{-3}$ m, $\lambda = 3^\circ$, $\alpha = 30^\circ$). The outer mean diameter of the nut is $d_n = 2.395 \times 10^{-2}$ m. The coefficient of friction is taken as a lubricated thread ($\mu_r = \mu_p = 0.15$). Using this information to achieve a pre-stress of 2676N the necessary tightening torque is 6.12N·m. Similarly, to achieve a pre-stress of 565N the necessary tightening torque is 1.29N·m.

Insertion of the inner crawler into the outer casing is shown in Fig. 9. To create motion of the inner crawler, the stacks need to be fired in a particular sequence. This is done by means of a controller.

3.2. Controller Design

A controller was designed to control the actuation of each stack. The controller was made with two modes: one for assembly, and one for actuating. The assembly mode, energized the braking stacks to allow insertion of the crawler into the outer casing. The

actuation mode was designed to fire each stack in a sequence that would cause the inner mechanism to linearly translate.

In actuating mode the waveforms supplied to the stacks were varied in frequency, amplitude, duty cycle and form. This was accomplished by using a PicStic 4x microprocessor that was programmed in the PicBasic language. The features of the microcontroller consist of: its two channel 12 bit digital to analog converter, its 8 bi-directional bit programmable high current input output lines and its high performance processor. In order to supply a voltage differential to the stacks to excite them a two-step power amplification circuit was designed. The first stage amplified the waveforms output by the PicStic using high accuracy instrumentation amplifiers. The amplifier design allows a very high bandwidth over a wide range of gains making it ideal for rapid data acquisition [39]. The amplifier gain is set using a single external resistor (R_G) and can range from 1 – 10,000. The gain, G , is given by

$$G = \frac{50k\Omega}{R_G} + 1 \quad (8)$$

For a chosen R_G value of 33k Ω the gain is 2.5. The output from the amplifier can then be further amplified by using a high voltage power amplifier.

Three model SA-10 high voltage power amplifiers and one SA-20 high voltage power supply were obtained from Sensor Technology Limited. The SA-10 is a two-channel high voltage power amplifier, it can be used as two individual ground referenced amplifiers providing a gain of 15, or a single bridged amplifier providing a gain of 30. Each channel gives a maximum ground referenced voltage variation of nominally 280 V

peak-to-peak. In bridged mode, the SA-10 provides a differential voltage variation of 560V [40]. During prototype testing the high voltage amplifiers and instrumentation amplifiers were configured to obtain a voltage of 285V across each stack. The diodes are used as a visual representation of the firing of each stacks, where R_1 is 333Ω . A picture of the circuit is shown in Fig. 10.

The actuating mode of the controller has two options. The first used square waves output from the PicStic that were then varied in amplitude, frequency and duty cycle. These waveforms were constructed using high and low logic levels cycled over chosen input-output pins of the PicStic. This firing sequence is intended to make the inner crawler move within the channel with a maximum controller frequency of 170Hz. The second actuation option uses a ramping waveform applied to the center stack.

From previous papers [33,34] it was discovered that ramping the signal of the center stack provided an increase in velocity of similar actuators when compared against the square wave signal at frequencies above 100Hz (due to less jarring motion). The ramping of the center stack was accomplished by using the digital to analog converter of the input-output coprocessor on the PicStic; to create four intermediate steps between the high and low voltage levels. Because the ramping function requires several intermediate steps, the maximum operating frequency of this signal is limited to 45Hz.

3.3. Prototype Results

The prototype was tested. The experimental and numerical results are presented in Table 4.

The quickest time the stacks can become charged (87% of maximum charge) or de-charged (13% of maximum charge) is 0.075s. Since there are six steps in each cycle of the actuator motion, the quickest time for one cycle of the inchworm movement is $6 \times 0.075\text{s} = 0.45\text{s}$. This corresponds to a maximum operating frequency of 2.22Hz. Multiplying this value by the extending stack displacement per step (7.2 μm) gives the theoretical actuator speed of 1.0mm/min. The difference in results between the model and the prototype differ by less than 9%, therefore validating the modeling and proof-of-concept demonstrator.

4. CONCLUSIONS

This paper investigates the design of an electrostrictive inchworm actuator. The design is based on its ability to maintain a locked position with no electrical power, fewer number of parts to reduce manufacturing complexity, and its adjustability. Parametric optimization design analysis of the brake assembly model were performed to select dimensions providing appropriate force/displacement characteristics.

To validate the computer model, a prototype was built. Frequency response (and actuator output speed) was limited in this case by the stack RC constant, however improvement in the stack design and manufacturing would increase the response speed of the actuator. The controller driving circuit has a maximum upper limit of 170Hz, whereas the limiting frequency of the inchworm cycle is 2.22Hz. Future work may be done to the stacks to enhance the maximum operational frequency and displacement. Moreover, the natural frequency of the actuator system may be investigated through future experimentation. At high frequencies, the ramping signal of the controller may also prove useful.

5. REFERENCES

- [1] K. Uchino, "Materials Issues in Design and Performance of Piezoelectric Actuators- An Overview", *Acta Materials*, Vol. 46, No. 11, pp3745-3753 , 1998.
- [2] K. L. Koudela and B. Hassier, "A 500Hz Mechanical Amplifier for use with Multilayered Piezoelectric Actuators," *Proceedings of The Ninth International Conference on Adaptive Structures and Technologies*, Boston, Massachusetts, U.S.A., p13-21, October 1998.
- [3] G. R. Lui, Z. Yili, K. Y. Lam, X. Q. Peng and J.Tani, "Finite Element Modelling of Piezoelectric Sensors and Actuators Bonded in Thick Composite Laminates," *Proceedings of The Eighth International Conference on Adaptive Structures and Technologies*, Wakayama, Japan, p113-122, October 1997.
- [4] D. R. Martinez, T. D. Hinnerichs and J. M. Redmond, "Vibration Control For Precision Manufacturing Using Piezoelectric Actuators," *Proceedings of The Sixth International Conference on Adaptive Structures and Technologies*, Rome, Italy, p3-22, October 1997.
- [5] B. Pletner and H. Abramovich, "Piezoelectric Sensors For Adaptive Suspensions," *Proceedings of The Sixth International Conference on Adaptive Structures and Technologies*, Rome, Italy, p404-417, October 1997.
- [6] Y. B. Cohen, S. Leary, M. Shahinpoor, J. O. Harrison and J. Smith, "Electro-Active Polymer (EAP) Actuators for Planetary Applications," *Proceedings of The SPIE Smart Structures and Materials*, Newport Beach, California, Vol. 3669, p57-63, March, 1999.

- [7] P. C. Hughes, W. G. Sincarsin and K. A. Carroll, "Trussarm-A Variable Geometry Truss Manipulator," Proceedings of The First Joint Japan/US Conference on Adaptive Structures, Nagoya, Japan, p715-725, November 1991.
- [8] S. Shao and Y. Murotsu, "Some Approaches to the Optimal Adaptive Geometries of Intelligent Truss Structures," Proceedings of The First Joint Japan/US Conference on Adaptive Structures, Nagoya, Japan, p743-771, November 1991.
- [9] K. Uchino, "Recent Development of Piezoelectric Actuators for Adaptive Structures," Proceedings of The Third International Conference on Adaptive Structures and Technologies, San Diego, California, U.S.A., p245-257, November 1992.
- [10] A. Benjeddou, M. A. Trindade and A. Ohayon, "A Finite Element Model for Shear Actuated Adaptive Structures," Proceedings of The Eighth International Conference on Adaptive Structures and Technologies, Wakayama, Japan, p133-142, October 1997.
- [11] M. E. Regelbrugge, and B. J. Huribut, "Developing of a Self-Sensing Multilayer Piezoceramic Actuator for Structural Damping Applications," Proceedings of The Fourth International Conference on Adaptive Structures and Technologies, Cologne, Federal Republic of Germany, p29-42, November 1993.
- [12] H. Janocha, D. J. Jendritza, and J. Schafer, "Active Damping of Forced Periodic Vibrations with Solid State Actuators," Proceedings of The Fourth International

Conference on Adaptive Structures and Technologies, Cologne, Federal Republic of Germany, p497-511, November 1993.

- [13] M. T. D'Eleuterio and G. B. Sincarsin, "Articulation Dynamics of Variable-Geometry Truss Structures", Proceedings of the Second Joint Japan/U.S. Conference on Adaptive Structures, Nov 12-14 1991, 1992, Nagoya, Japan, p 621.
- [14] R. Stibitz, "Incremental Feed Mechanisms", U.S. Patent: 3,138,749, 1964.
- [15] M. McNancy, "Inchworin actuator", U.S. Patent: 5,3323,942, 1994.
- [16] K. Hsu and A. Biatter, "Transducer", U.S. Patent: 3,292,019, 1966.
- [17] G.L. Locher, "Micrometric linear actuator", U.S. Patent: 3,296,467, 1967.
- [18] A.D. Brisbane, "Position control device", U.S. Patent: 3,377,489, 1968.
- [19] G. V. Galutva, "Device for precision displacement of a solid body", 1987.
- [20] R. A. Bizzigotti, "Electromechanical translational apparatus". US. Patent: 3,902,085, 1975.
- [21] Y. Sakitani, "Stepwise fine adjustment", U.S. Patent: 3,952,215, 1976.
- [22] M. Ishikawa and Y. Sakitani, "Two-directional piezoelectric driven fine adjustment device", U.S. Patent: 4,163,168, 1979.
- [23] G. O'Neill, "Electromotive actuator", U.S. Patent: 4,219,755, 1980.

- [24] T. Taniguchi, "Piezoelectric driving apparatus", US Patent: 4,454,441, 1984.
- [25] A. Hara, H. Takao, Y. Kunio, T. Sadayuki and N. Keiji, "Electromechanical translation device comprising an electrostrictive drive of a stacked ceramic capacitor type", U.S. Patent: 4,570,096, 1986.
- [26] C. W. Staufenberg and R. J. Hubbell, "Piezoelectric electromechanical translation apparatus", U.S. Patent: 4,622,483, 1986.
- [27] T. Fujimoto, "Piezo-electric actuator and stepping device using same", U.S. Patent: 4,714,855, 1987.
- [28] T. Murata, "Drive apparatus and motor unit using the same", U.S. Patent: 4,974,077, 1990.
- [29] S. Shibuta, Y. Morino, Y. Shibayama and K. Sekine, "Adaptive Control of Space Truss Structures by Piezoelectric Actuator", Tsukuba Space Cent Source: Jt Japan/US Conference on Adaptive Structures, Proceedings of the Second Joint Japan/U.S. Conference on Adaptive Structures, Nov 12-14 1991, 1992, Nagoya, Japan Sponsored by: PA, Publ by Technomic Publ Co Inc, Lancaster, USA, p 245.
- [30] G. Rennex, "Inchworm actuator", U.S. Patent: 5,332,942, 1994.
- [31] T. Pandell and E. Garcia, "Design of a piezoelectric caterpillar motor" Proceedings of the ASME aerospace division, AD-Vol. 52, p. 627-648, 1996.

- [32] T. P. Galante, “Design and Fabrication of a High Authority Linear Piezoceramic Actuator: The PSU H3 Inchworm”, The Pennsylvania State University: Graduate School, Department of Mechanical Engineering, August 1997.
- [33] S. Canfield, S. Edinger, B. M. Frecker, and G. Koopmann, “Design of Piezoelectric Inchworm Actuator and Compliant End-Effect for Minimally Invasive Surgery”, Society of Photo-Optical Instrumentation Engineers, p 835-843, Part of the SPIE Conference on Smart Structures and Integrated Systems, Newport Beach California, March 1999.
- [34] J. Frank, G. Koopmann, W. Chen and G. A. Lesieutre, “Design and Performance of a High Force Piezoelectric Inchworm Motor”, Proceedings of SPIE - The International Society for Optical Engineering , v 3668, n II, Proceedings of the 1999 Smart Structures and Materials - Smart Structures and Integrated Systems, 1999, Society of Photo-Optical Instrumentation Engineers, Bellingham, WA, USA, p 717-723.
- [35] Sensor Technology Limited, www.sensortech.ca , 2001.
- [36] V. Giurgiutiu and C. A. Rogers, “Energy-Based Comparison of High-Power Commercially-Available Induced-Strain-State Actuators,” Proceedings of The Sixth International Conference on Adaptive Structures and Technologies, Rome, Italy, p113-130, October 1997.
- [37] J.E. Shigley and C.R. Mishcke, Mechanical Engineering Design, 5th Edition, McGraw-Hill Book. Co. 1989.

- [38] Vishay Measurements Group, Inc., 2001,
<http://www.measurementsgroup.com/guide/glossary/vonmises.htm>, (Aug. 2001).
- [39] Analog Devices, “High Accuracy 8-pin Instrumentation Amplifier – AMP02”,
Rev. D, Norwood MA USA.
- [40] Sensor Technology Limited “SA-10 High-Voltage Power Amplifier Technical
Manual”, Rev. 2, March 23, 2000.

Table 1 - Actuator design specifications

Actuator Specifications	
Minimum Displacement (mm)	15
Minimum Force Output (N)	20
Maximum Operating Voltage (V)	200

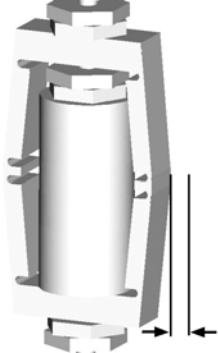
Table 2 - Comparison of free displacement of BM500 and BM600

	PZT		PMN	
	Ansys	Exp	Ansys	Exp
Free Displacement (um)	7.2	7.3	30.0	28.8

Table 3 Actuator output force

Brake Pad Clearance (um)	Actuator Output Force (N)	
	Ti on Steel	Ti on Ti
0	112	65
25.4	84	48
50.8	54	32
76.2	25	15

Table 4 - Summary of inchworm actuator results

Inchworm Actuator Results	Ansys Design Model	Ansys Prototype Model	Measured from Prototype
Brake Stack Free Disp. (um) 	30.0	27.1	26.0
Brake Pad Disp. (um) 	107.4	78.2	71.1
Extending Stack Free Disp. (um) 	39.9	16.7	16.0
Brake Pad Blocked Force (N): 25.4 Clearance 50.8 Clearance	64.2 41.6	18.6 7.5	---
Actuator Output Force (N): 25.4 Clearance 50.8 Clearance	83.5 54.0	24.2 10.0	15.1
Max. Operating Freq. (Hz) Actuator Speed (mm/min)	--- ---	2.22 1.0	0.33 0.2

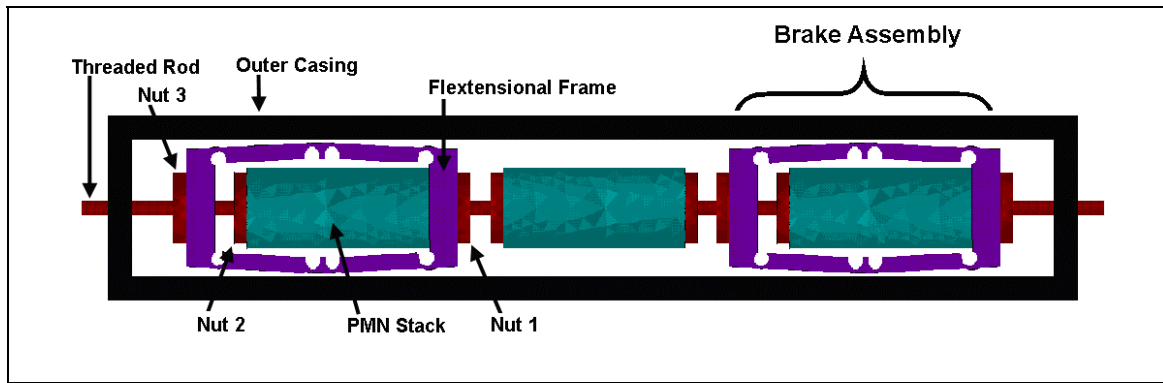


Figure 1 – The proposed electrostrictive inchworm actuator concept

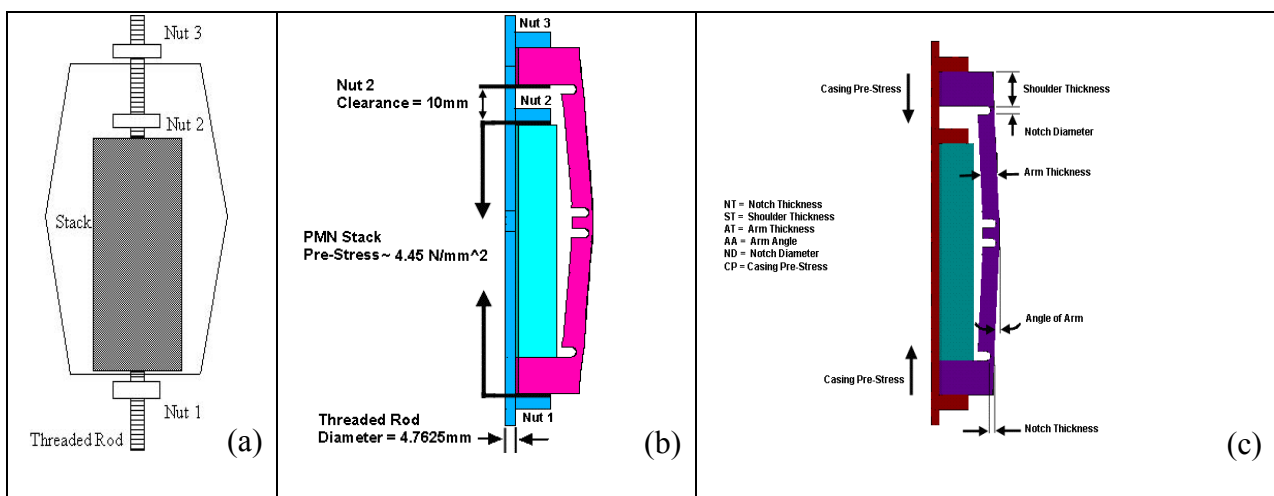


Figure 2 – (a) Schematic of the flextensional frame and stack with pre-tension nuts; (b) The actuator fixed dimensions; and (c) the actuator free dimensions

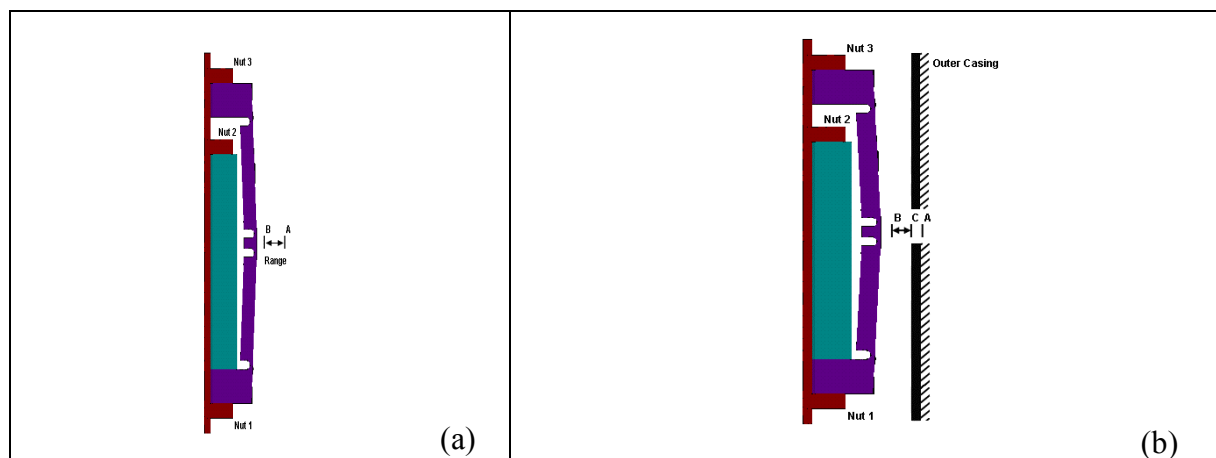


Figure 3- (a) The brake assembly range; and (b) the contact with outer casing

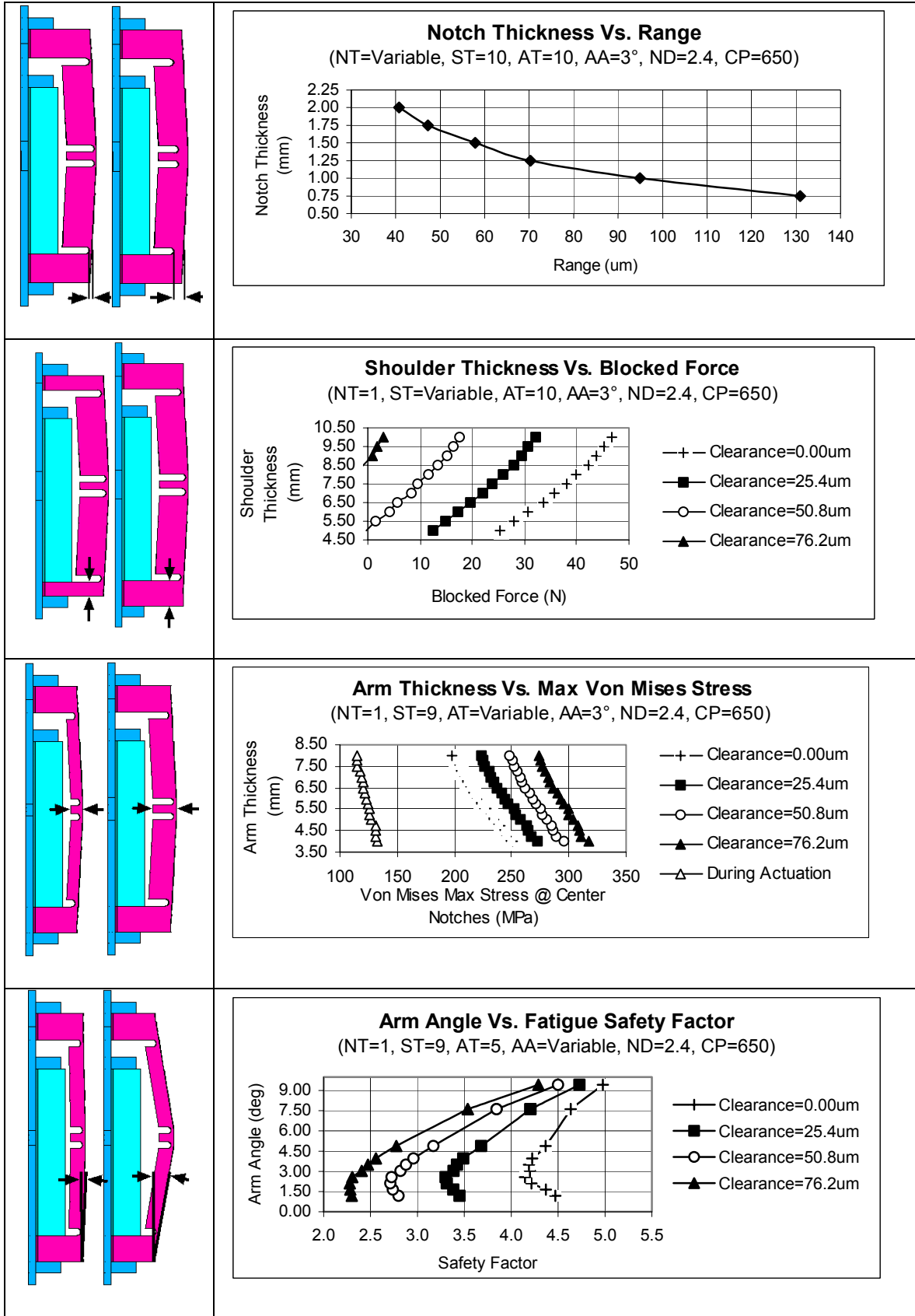


Figure 4 – Parametric design optimization of free dimension design parameters

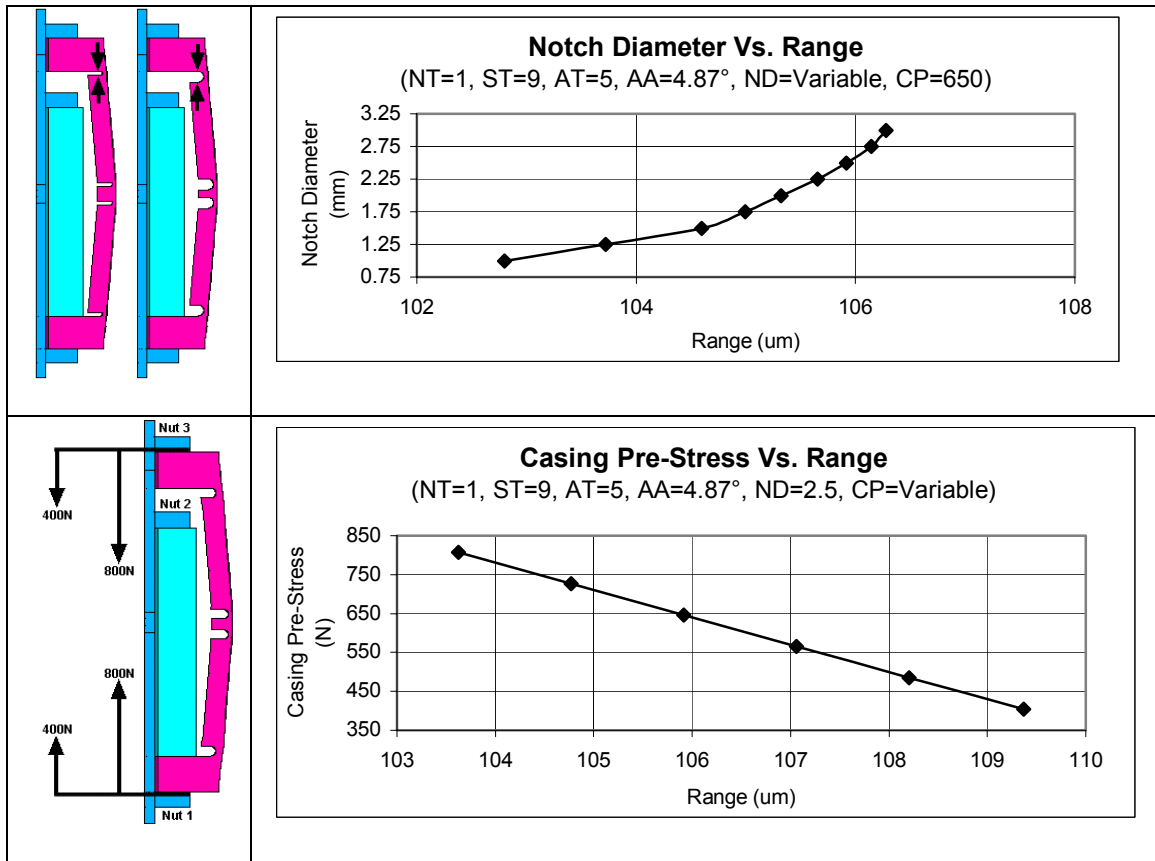


Figure 5 - Variation of notch diameter and casing pre-stress with free dimension design parameters

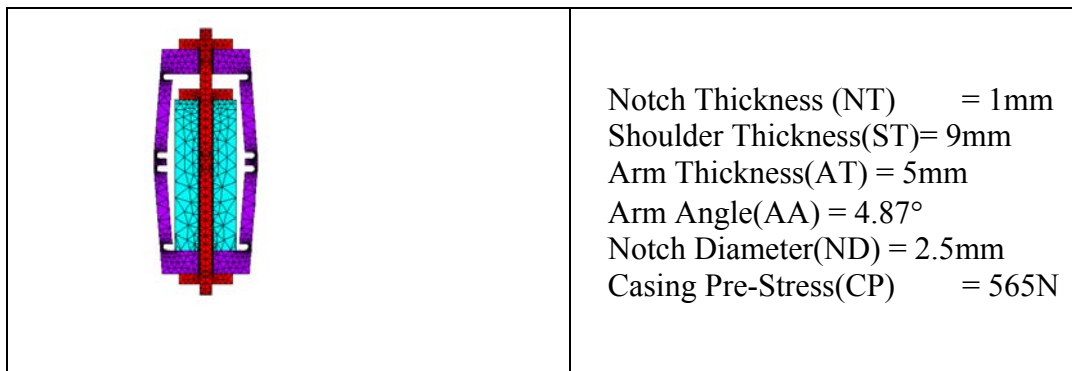


Figure 6 - Final design modeling results

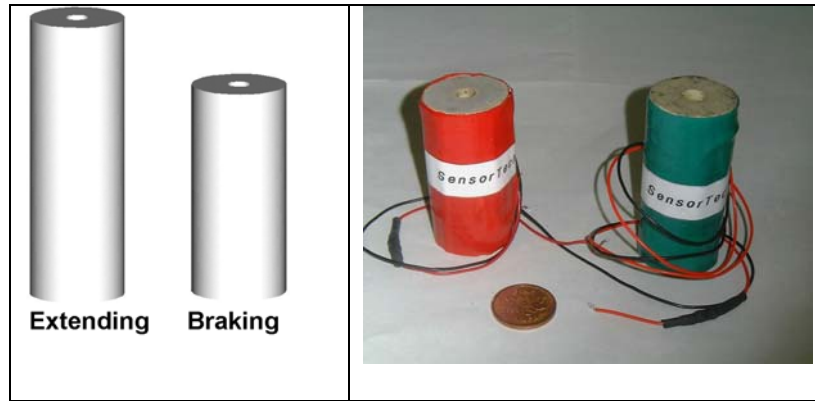


Figure 7 - Design and prototype stacks

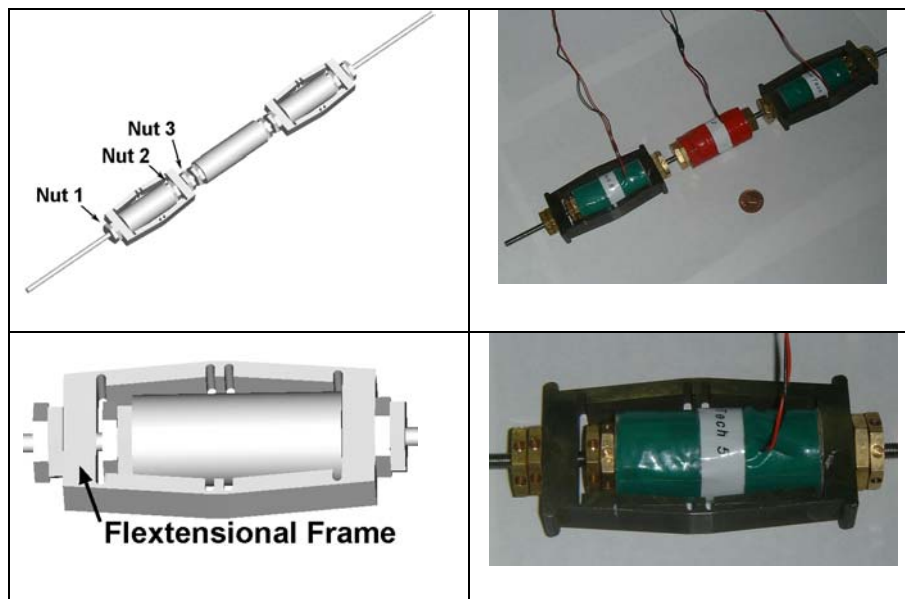


Figure 8 – Flextensional frame and the inner crawler

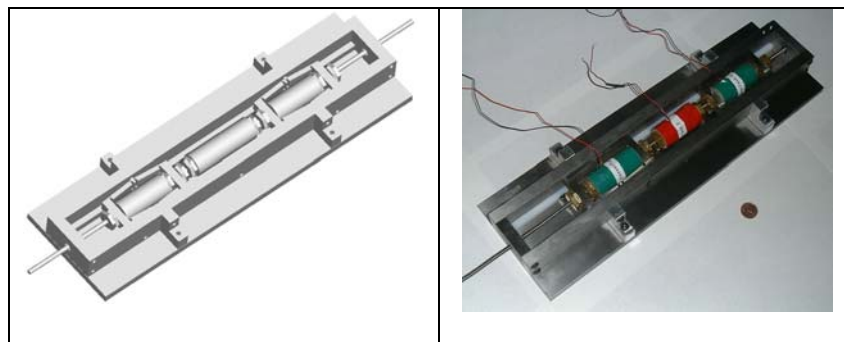


Figure 9 - Assembly of outer casing and inner crawler

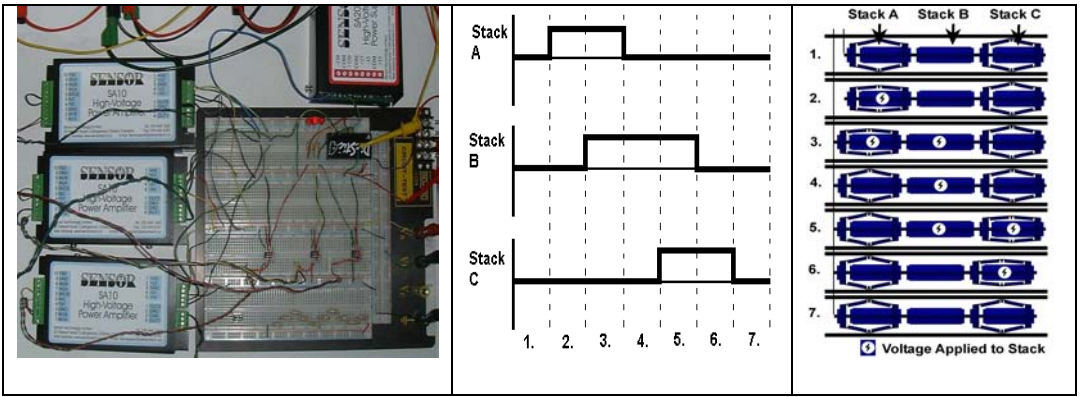


Figure 10 - Controller assembly and waveforms